HYDROLYSIS MECHANISM OF RUTHENIUM(III) ANTICANCER COMPLEXES

4.1 Introduction

Attempts to find a new metal based anticancer drugs except platinum, number ruthenium complexes have recently been investigated for their antitumor activity.[1-4] In particular, Keppler type complexes (HL)[*trans*-$RuCl_4L_2$](L= heterocyclic nitrogen ligand) and related tetrachlororuthenium(III) DMSO complexes of the type (X)[*trans*-$RuCl_4$(DMSO)L] (L=imidazole; X= Na or HL) such as NAMI or NAMI-A exhibit remarkable antimetastatic properties (discussed in chapter 3). Extensive researches on the chemical properties and effects of these ruthenium complexes on the cellular level have been done[5-8] but definite mechanism of action is yet been understood. Furthermore, no clear structure-activity relationship (SAR) has been established. For platinum based anticancer complexes like cisplatin, carboplatin etc, hydrolysis process has been proven to be a key activation step before reaching its intracellular target[9,10] because aqua complexes are much more reactive toward biomolecules than the parent chloro complexes.[11-13] Experimental studies on ruthenium complexes also suggest similar activation at physiological condition.[14] These ruthenium(III) complexes (NAMI-A[15-17], KP1019[18] and [Him][*trans*-$RuCl_4(im)_2$] (ICR) etc.[18-20]) are relatively labile, undergoing hydrolysis to the corresponding more reactive aquated form. In other word, they appear to be prodrugs that on hydrolysis *in vivo* form a number of potentially active species.[5,6] Therefore, a proper investigation on hydrolytic properties of these type of complexes are very important in order to understand the nature of the active species that could be useful to optimize the protocols for the administration of the drugs.

In comparison with the experimental efforts, theoretical studies regarding the action mode of ruthenium anticancer complexes at the *ab initio* quantum-mechanical (QM) level are still very less.[21,22] In a recent DFT study, Chen *et. al*. have investigated the hydrolysis mechanism of a series of ruthenium(III) complexes including NAMI-A and ICR.[23-27] In addition, deeper insight into the aquation of the NAMI-A and ICR are further explored by Besker *et. al*. and Vargiu *et. al*. using DFT-PB and DFT-PCM methods.[28,29] However, the indazole and triazole analogues have possessed different structural characteristics. Therefore, theoretical studies on the hydrolytic properties of

these complexes are very important at the molecular level for understanding the mode of action and revealing the structure-activity relationship (SAR).

In this study, we have carried out a systematic investigation on hydrolyses of two ruthenium complexes **II** and **IV** (scheme 1) using combined density functional theory (DFT) calculation and an implicit description of the solvent through the conductor-like polarizable continuum model (CPCM).[30] In this hydrolysis mechanism we have mainly focused on Cl^- and DMSO dissociation up to second aquation since poly-oxo species are rapidly formed during the second hydrolysis which involves in interaction with tumor cells.

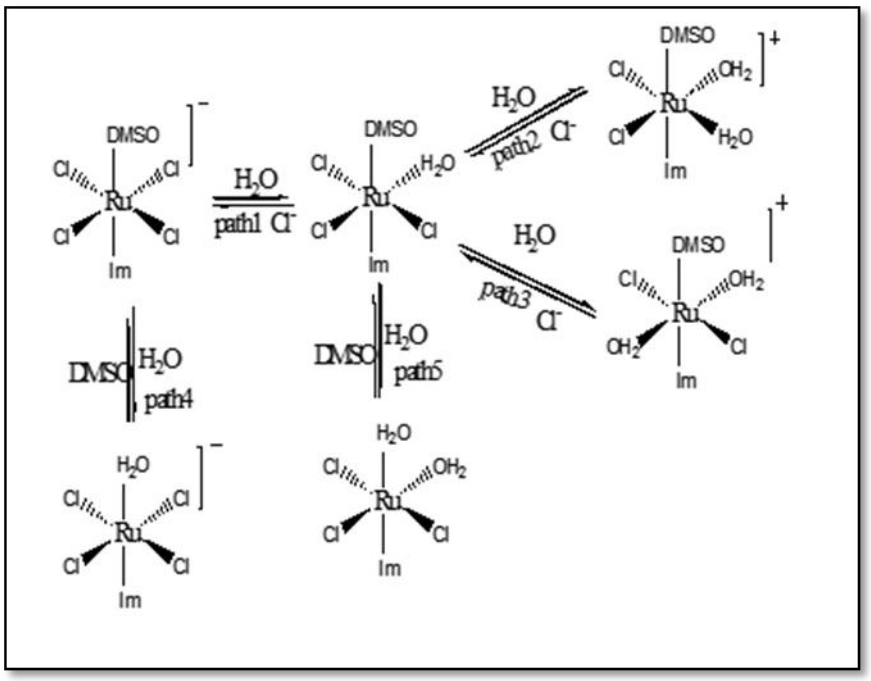

Scheme1 Proposed hydrolysis mechanism of ruthenium(III) complex

4. 2 Computational Details

Hydrolysis mechanism of ruthenium(III) complexes have been carried out in the framework of the density functional theory, employing the Gaussian 09 package.[31] Full in *vacuo* optimization without imposing any symmetry constraint on the intermediates and transition states have been done using the B3LYP[32] exchange-correlation functional with 6-31G(d,p)[33] basis set on N, S, C, O, H and Cl atoms and LANL2DZ[34] basis set on Ru atom. A vibrational analysis at the same level of theory is performed to ensure that optimized structures are local minima or transition state and to estimate zero-point vibrational energy and thermal and entropic corrections.

The transition states are also confirmed by intrinsic reaction coordinate (IRC) calculations.[35,36] Single-point energies are computed on optimized structures using a higher basis set of LanL2DZ (on Ru atom), 6-311+G(d, p) (on H, C, N, O atoms) and 6-311+G(3d) (on Cl, S atoms) in *vacuo* and in solvent medium using implicit solvation model CPCM to obtain an improved value of the internal energy.[37-39]

Gibbs free energies and enthalpies are computed with the following equations:[23]

$$G_{solv} = G_{solvent} - G_{gas}$$

$$H(aq) = E_{ZPE}(g) + G_{solv} + H_{therm}\ (g)$$

$$G(aq) = E_{ZPE}(g) + G_{solv} + G_{therm}(g)$$

Where G_{solv} is the solvation free energy, $G_{solvent}$ is the Gibbs free energy in solvent medium, G_{gas} is the Gibbs free energy in gas phase, $H(aq)$ is the enthalpy and $G(aq)$ is the Gibbs free energy in aqueous medium, $H_{therm}(g)$ is the thermal correction to enthalpy and $G_{therm}(g)$ is the thermal correction to Gibbs free energy in the gas phase.

4.3 Results and Discussion

4.3.1 Structural characteristics of the species involved in Cl^- hydrolysis

The gas phase optimized structures of all the species involved in first step of Cl^- hydrolysis of complexes **II** and **IV (**path1**)** are shown in Fig. 4.1 and those in the second step of the hydrolysis (path 2 and path 3) are depicted in Fig. 4.2. The calculated significant geometrical parameters of the optimized stationary points are listed in Table 4.1 and 4.2 and important optimized geometries presented in Fig. 4.1 and 4.2. From the Table 4.1 and Table 4.2 and Fig. 4.1 and Fig. 4.2, quite a numbers of geometrical variations in the structure of reactants, products and intermediates are noticed and only the important ones are discussed in detail. Ruthenium complexes (**II** and **IV**) and their hydrolyzed products attain pseudo-octahedral geometry around the central ruthenium atom. Aqua ligand in the hydrolyzed product forms hydrogen bonding with Cl^- or DMSO ligand

4.3.1.1 First hydrolysis step

Geometrical parameters of complexes **II** and **IV** have already discussed in Table 3.1 in chapter 3. Table 4.1 summarized the geometrical parameters of first step of Cl^- hydrolysis. It has been observed from Table 4.1 that in the first intermediate, **II-1**, the incoming water molecule forms hydrogen bonding with two adjacent chloro ligand at distances of 2.31Å (Cl4−HOH) and 2.28 Å.

Table 4.1 Selected bond lengths (Å) and bond angles (^{0}) calculated for all stationary points in the first step of Cl^- hydrolysis for the complexes **II** and **IV**.

Parameters	Complex **II**				Complex **IV**			
	II-1	**TSII-1**	**II-2**	**II-a**	**IV-1**	**TSIV-1**	**IV-2**	**IV-a**
Ru—Cl1	2.43	3.72			2.38	3.00		
Ru—Cl2	2.41	2.37	2.42	2.37	2.46	2.57	2.44	2.38
Ru—Cl3	2.44	2.35	2.41	2.34	2.48	2.42	2.43	2.37
Ru—Cl4	2.46	2.37	2.40	2.45	2.42	2.40	2.37	2.41
Ru—O(wat)	4.06	3.28	2.10	2.20		2.53	2.13	2.18
Ru—S	2.41	2.45	2.35	2.36	2.40	2.42	2.37	2.36
Ru—N	2.11	2.11	2.10	2.11	2.10	2.10	2.10	2.08
N—Ru—S	177.3	177.4	178.3	177.3	176.9	175.9	174.0	175.3
Cl1—Ru—Cl2	89.7	88.6			90.8			
Cl2—Ru—Cl3	90.4	93.5	91.3	97.3	87.9	82.0	89.9	94.5
Cl3—Ru—Cl4	89.4	96.3	92.3	96.5	89.5	84.5	91.7	94.9
Cl4—Ru—Cl1	90.5	81.6			91.8	76.2		
Cl4—Ru—O			88.9	81.3			91.8	83.3
Cl1—Ru—O		51.9				61.8		
O—Ru—Cl2		72.8	87.5	86.9		69.6	86.6	87.3

(Cl1−HOH), while in intermediate **IV-1**, hydrogen bonds are formed at a distance of 2.48 Å (Cl4−HOH) and 2.45 Å (Cl1−HOH). The transition states (**TSII-1** and **TSIV-1**) found for the first hydrolysis step of complexes **II** and **IV** is confirmed by presence of one imaginary frequency each having pentagonal bipyramidal geometry. The distance between Ru^{3+} ion and O atom of the incoming water molecule reduces from 4.06 Å in **II-1** to 3.28 Å in **TSII-1** and from 4.29 Å in **IV-1** to 2.53 Å in **TSIV-1**,

while, Ru—Cl distance increases from 2.38 Å to 3.72 Å in **TSII-1**, and from 2.37 Å to 3.00 Å in case of **TSIV-1**. That is, in both the complexes (**II** and **IV**), formation Ru—O(wat) bond and breaking of Ru—Cl bond take place same time simultaneously exhibiting interchange dissociative mechanism. In the intermediates **II-2** and **IV-2**, the Cl^- ligand has been completely replaced with H_2O molecule and forms a bond with Ru^{3+} ion at distance of 2.11 Å and 2.13 Å, respectively. On the other hand, the leaving Cl^- ligand forms intermolecular hydrogen bonding with H atom of the coordinated water molecule at distance of 1.92 Å in **II-2** and 1.87 Å in **IV-2**. The hydrolysis products **II-a** and **IV-a** acquire pseudooctahedral geometry, in which the leaving Cl^- ligand is being removed completely with water molecule which forms a hydrogen bonding with O atom of DMSO molecule at a distance of 1.86 Å.

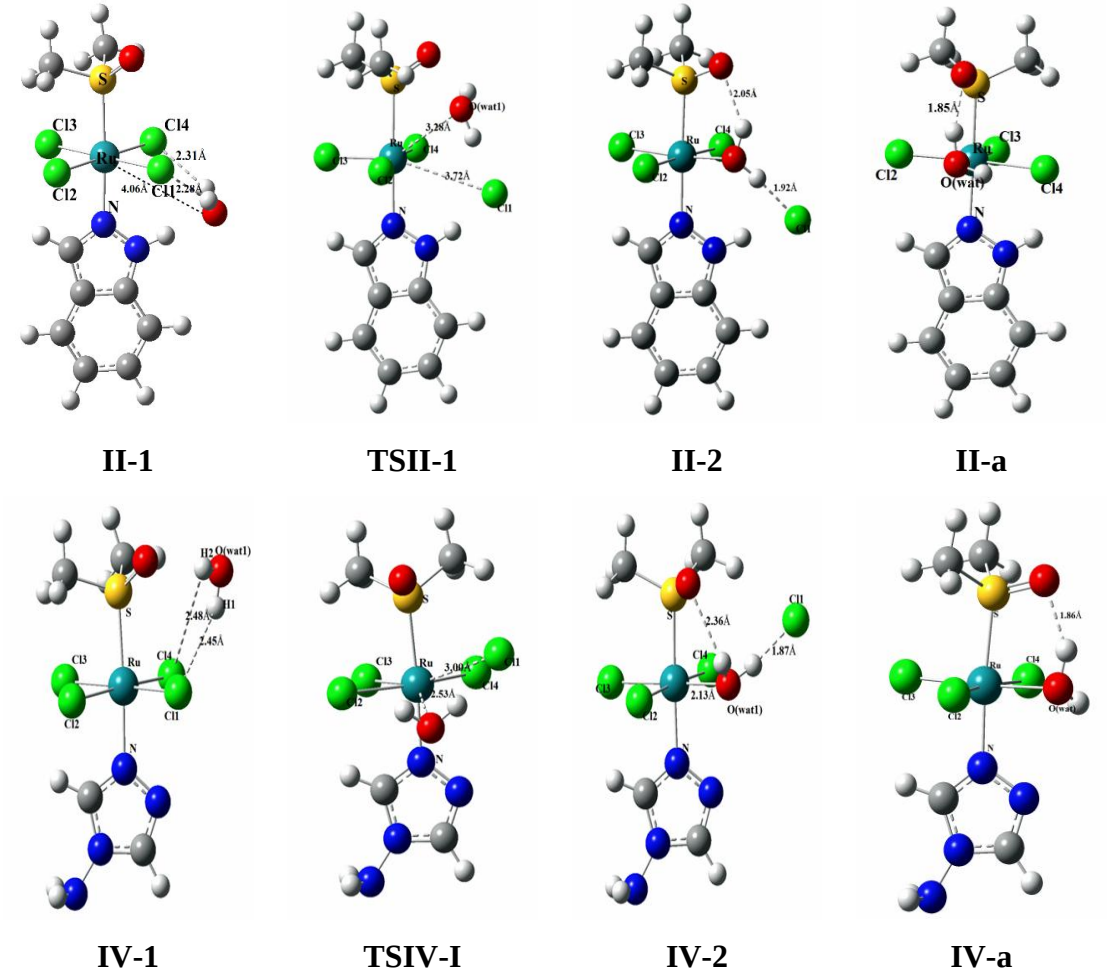

Fig.4.1 Optimized structures for the species involved in the first step of Cl^- hydrolysis of complex **II** and **IV** (path 1).

4. 3.1.2 Second step of hydrolysis

The optimized geometrical parameters evaluated by DFT for hydrolysis of mono aqua ruthenium complexes **II-a** and **IV-a** are listed in Table 4.2 and geometries are shown in Fig. 4.2. In this study, two paths are depicted for the second hydrolysis of ruthenium complexes: path 2 corresponds to the replacement of Cl^- ligand *cis* to the first coordinated water molecule and path 3 corresponds to the replacement of Cl^- ligand *trans* to the first coordinated water molecule from **II-a** and **IV-a** complexes. In the path 2, **II-3** exhibits two hydrogen bonds (Cl3−HOH= 2.67 Å, Cl4−HOH= 2.69 Å) resulting from the interaction of entering water molecule with two adjacent Cl^- ligands (Fig. 4.2). Similar types of hydrogen bonding interactions have been exhibited by the intermediate **IV-3** at distances 2.62 Å (Cl3−HOH) and 2.44 Å (Cl4−HOH). The geometry of transition states, **TSII-2** and **TSIV-2** reveal an interchange dissociative rather than associative character. In both the cases the entering water molecule approaches the metal center and form Ru−O bond before complete removal of Cl^- ligand from the ruthenium ion. The structures of **TSII-2** and **TSIV-2** are found to be similar to that of **TSII-1** and **TSIV-1**, that is, the bond length Ru−O(wat2) reduces and the Ru-Cl4 distance correspondingly increases. In the intermediates **II-4** and **IV-4** the bond lengths Ru−O(wat2) are found to be in the range of 2.11-2.19 Å whereas the leaving Cl^- ligand lies at distances of 3.97 Å and 3.99 Å from the ruthenium coordination center. Further, it is noted that the expelled Cl^- ligand forms two hydrogen bonds with the two coordinated water molecules (Fig. 4.2). *cis*-diaquated products **II-b** and **IV-b** obtained due second hydrolysis of complexes **II** and **IV** proceed through path 2 show pseudooctahedral geometry. Similar geometrical parameters are observed for the stationary points obtained, proceed through path 3 (Fig 4.2 and Table 4.2) .

Table 4.2 Selected bond lengths (Å) and bond angles (^{0}) calculated for all stationary points in the second step of Cl^- hydrolysis of complex **II** and **IV**

Parameters	Complex **II**								Complex **IV**							
	Path2				Path3				Path2				Path3			
	II-3	**TSII-2**	**II-4**	**II-b**	**II-3′**	**TSII-2′**	**II-4′**	**II-b′**	**IV-3**	**TSIV-2**	**IV-4**	**IV-b**	**IV-3′**	**TSIV-2′**	**IV-4′**	**IV-b′**
Ru—Cl2	2.37	2.35	2.34	2.29	2.37	2.39	2.36	2.39	2.38	2.37	2.38	2.35	2.38	2.39	2.35	2.37
Ru—Cl3	2.35	2.41	2.37	2.36	2.35	3.08	4.19		2.38	2.41	2.36	2.31	2.38	3.04	4.32	
Ru—Cl4	2.46	2.88	3.97		2.46	2.55	2.43	2.40	2.42	2.78	3.99		2.42	2.51	2.41	2.37
Ru—O(W1)	2.19	2.20	2.12	2.16	2.19	2.16	2.16	2.14	2.17	2.23	2.16	2.19	2.17	2.12	2.11	2.05
Ru—O(W2)		2.72	2.19	2.24		2.28	2.03	2.03	4.29	2.68	2.11	2.17	4.29	2.39	2.11	2.18
Ru—S	2.38	2.41	2.38	2.41	2.38	2.36	2.42	2.39	2.38	2.37	2.36	2.37	2.38	2.39	2.38	2.41
Ru—N	2.11	2.11	2.10	2.09	2.11	2.11	2.11	2.11	2.08	2.08	2.11	2.11	2.08	2.09	2.08	2.10
N—Ru—S	175.5	173.9	177.1	174.3	175.5	176.5	174.3	174.1	174.2		176.1	177.0	174.1	170.4	170.7	167.1
Cl2—Ru—O(W1)	86.2	81.1	92.1	91.9	86.2	78.8	89.1	89.1	86.7	78.0	87.8	88.9		81.5	93.2	98.9
Cl2—Ru—Cl3	95.6	87.3	97.1	99.0	95.6				93.1	85.2	95.7	98.9	93.5	75.3		
Cl3—Ru—Cl4	95.1		84.6		95.1				95.5				95.4	123.2		
Cl4—Ru—O(W1)	83.1	67.8			83.1		84.4		84.7	67.9			84.9	79.1		
O(W2)—Ru—O(W1)			86.2	85.1							88.3	80.4				
Cl4—Ru—O(W2)		62.9					93.0			63.9						
Cl3—Ru—O(W2)				84.3			93.5					92.4			85.9	
Cl2—Ru—O(W2)								93.5	89.9						91.5	83.5

Path 2

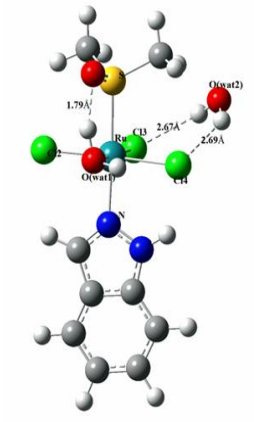

II-3

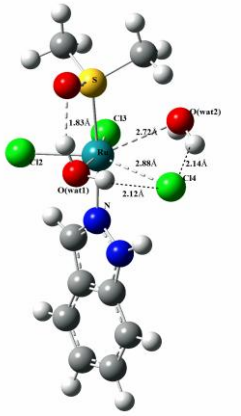

TSII-2

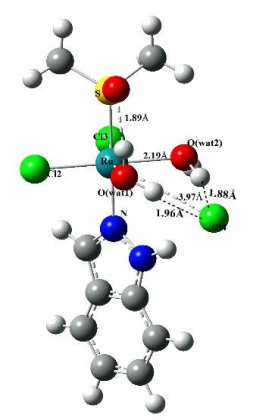

II-4

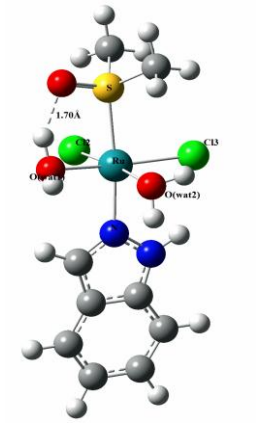

II-b

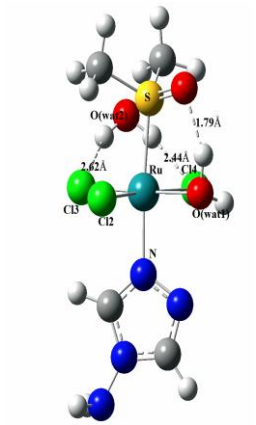

IV-3

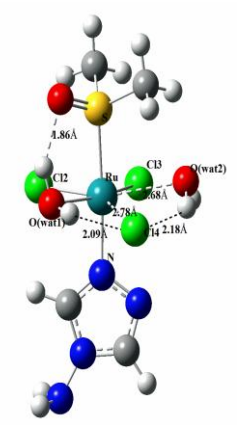

TSIV-2

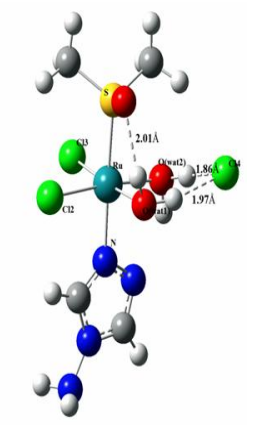

IV-4

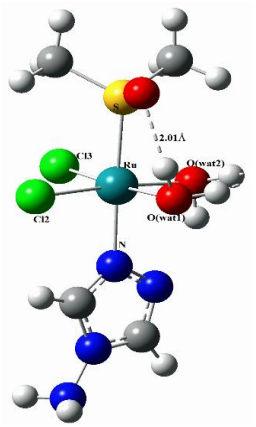

IV-b

Path 3

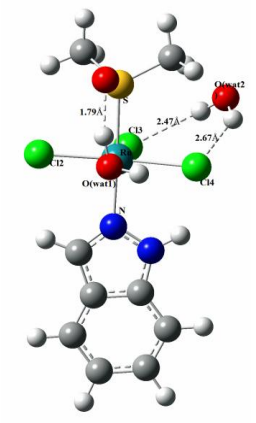

II-3/

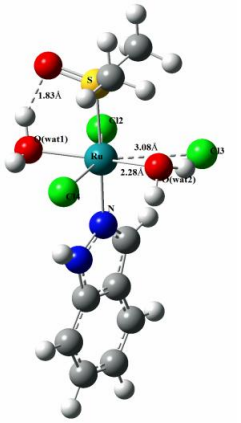

TSII-2/

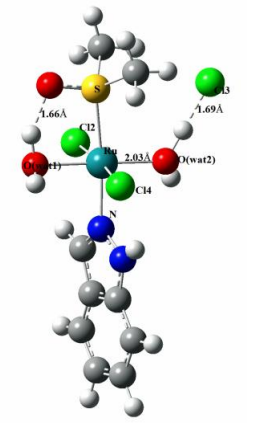

II-4/

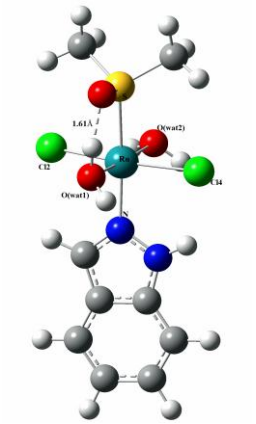

II-b/

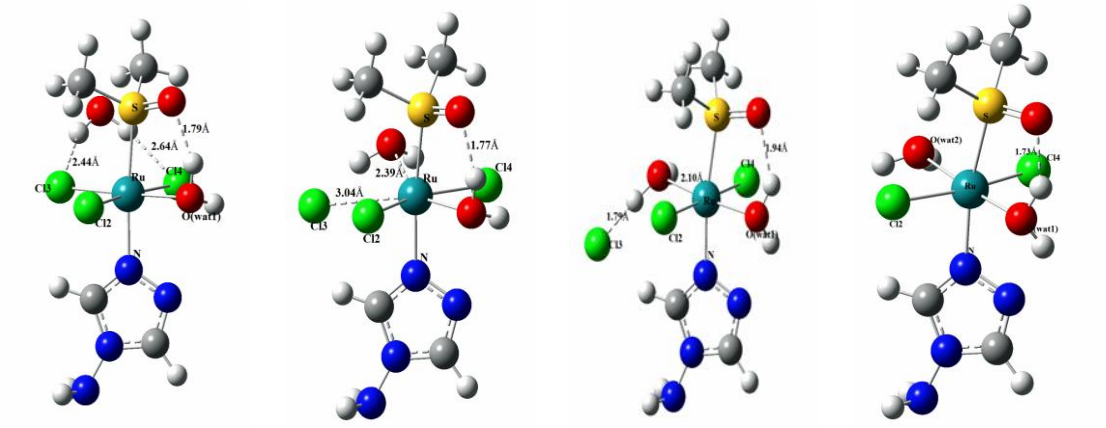

IV-3′ **TSIV-2′** **IV-4′** **IV-b′**

Fig.4.2 Optimized structures for the species involved in the second step of Cl^- hydrolysis of complex **II** and **IV** (path 2 and 3).

4.3.2 Structural characteristics for the species involved in DMSO hydrolysis

Geometrical parameters of the stationary points involved in the hydrolysis of DMSO group proceed through paths 4 and 5 are summarized in Table 4.3 and Table 4.4 and optimized structures are shown in Fig. 4.3 and 4.4. In intermediate **II-5** the incoming water molecule is stabilized by a hydrogen bonding network. The hydrogen bonding distance between oxygen atom of leaving DMSO molecule and hydrogen atom of water molecule calculated to be 2.07 Å, however, no hydrogen bonding is observed in intermediate **IV-5** (Fig. 4.3). The transition states **TSII-3**, **TSIV-3** are characterized by presence of one imaginary frequency each. The data reported in Fig. 4.3 and Table 4.3 reveal that in the TS, the Ru−S(DMSO) bond breaks and Ru−O (water) bond forms. Further, both the TS structures follow an interchange dissociative mechanism like that of the TS structures involved in Cl^- hydrolysis. In the optimized intermediates **II-6** and **IV-6**, the entering incoming water molecule replaces the DMSO molecule, which is moved far away from the ruthenium center, shown by the Ru−O=2.21 Å and Ru−S of DMSO=5.28 Å in case of **II-6** while, Ru−O= 2.17 Å and Ru−S of DMSO=4.43 Å in case of **IV-6**. The optimized stationary points for the path 5 are quite similar with that of the path 4 and also show similar hydrogen bond pattern.

Table 4.3 Selected bond lengths (Å) and bond angles (^{0}) calculated for all stationary points in the first step of DMSO hydrolysis of complex **II** and **IV**.

Parameters	Complex **II**				Complex **IV**			
	II-5	**TSII-3**	**II-6**	**II-c**	**IV-5**	**TSIV-3**	**IV-6**	**IV-c**
Ru—Cl1	2.39	2.42	2.43	2.44	2.38	2.41	2.41	2.42
Ru—Cl2	2.42	2.38	2.40	2.39	2.46	2.47	2.47	2.45
Ru—Cl3	2.44	2.42	2.40	2.39	2.48	2.37	2.48	2.47
Ru—Cl4	2.49	2.48	2.48	2.49	2.42	2.41	2.38	2.41
Ru—O(wat)	4.27	3.06	2.21	2.21	4.28	3.10	2.17	2.18
Ru—S	2.39	3.42	5.28		2.40	3.49	4.43	
Ru—N	2.12	2.02	2.06	2.06	2.10	2.00	2.06	2.06
N—Ru—S	178.5	150.2	152.5		176.9	148.0	125.2	
Cl1—Ru—Cl2	91.7	91.6	90.6	90.6	90.8	90.9	89.1	89.1
Cl2—Ru—Cl3	91.4	90.6	91.5	92.4	87.9	82.0	87.3	87.4
Cl3—Ru—Cl4	88.3	89.3	88.9	88.7	89.5	84.5	90.7	90.3
Cl4—Ru—Cl1	88.5	88.5	88.6	88.1	91.7	76.2	92.8	92.6
S—Ru—O	52.7	39.6	31.8		52.6	51.9	55.1	
O—Ru—N		156.3	175.7	175.2		159.8	177.9	177.9

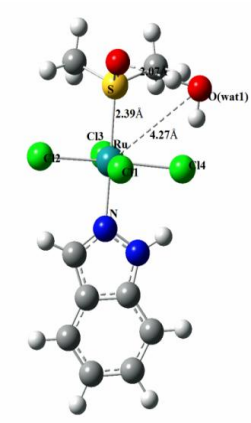

II-5

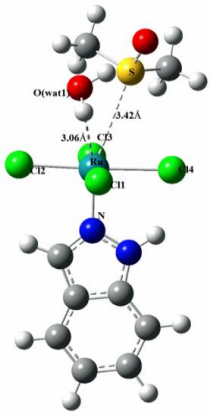

TSII-3

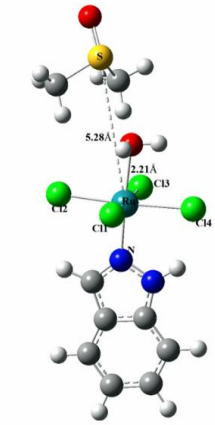

II-6

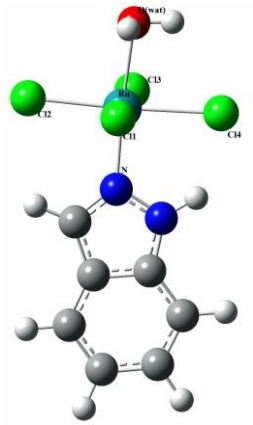

II-c

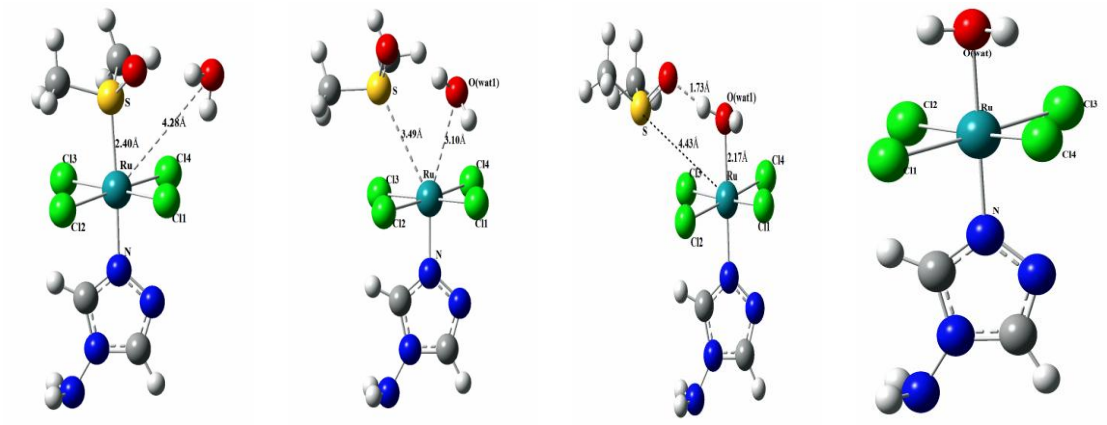

IV-5 **TSIV-3** **IV-6** **IV-c**

Fig.4.3 Optimized structures for the species involved in the first DMSO hydrolysis of complex **II** and **IV** (path 4).

Table 4.4 Selected bond lengths (Å) and bond angles (^{0}) calculated for all stationary points in the second step of DMSO hydrolysis of complex **II** and **IV**.

Parameters	Complex **II**				Complex **IV**			
	II-7	**TSII-4**	**II-8**	**II-d**	**IV-7**	**TSIV-4**	**IV-8**	**IV-d**
Ru—O(wat1)	2.20	2.18	2.21	2.21	2.17	2.15	2.19	2.18
Ru—Cl2	2.38	2.37	2.37	2.37	2.38	2.37	2.39	2.38
Ru—Cl3	2.34	2.34	2.32	2.34	2.48	2.37	2.36	2.37
Ru—Cl4	2.45	2.45	2.49	2.45	2.42	2.41	2.42	2.42
Ru—O(wat2)	4.61	2.19	2.10	2.08	4.29	2.88	2.13	2.13
Ru—S	2.37	3.56	2.35		2.38	3.55	4.41	
Ru—N	2.11	2.02	2.10	2.10	2.08	1.99	2.07	2.08
N—Ru—S	177.3	153.9			176.9	154.9	-	-
O(wat1)—Ru—Cl2	87.0	87.8	87.2	87.2	86.7	87.2	87.9	87.8
Cl2—Ru—Cl3	96.9	95.8	96.5	97.3	93.1	93.7	95.8	95.5
Cl3—Ru—Cl4	94.6	94.2	95.5	95.5	95.4	93.3	94.7	94.7
Cl4—Ru—O(wat1)	81.5	81.9	79.8	81.0	84.9	85.4	81.7	81.7
S—Ru—O(wat2)	49.6	56.9	55.4	55.4	71.2	57.6	54.7	54.7
O(wat2)—Ru—N	-	148.2	176.3	177.4	-	146.7	176.6	176.8

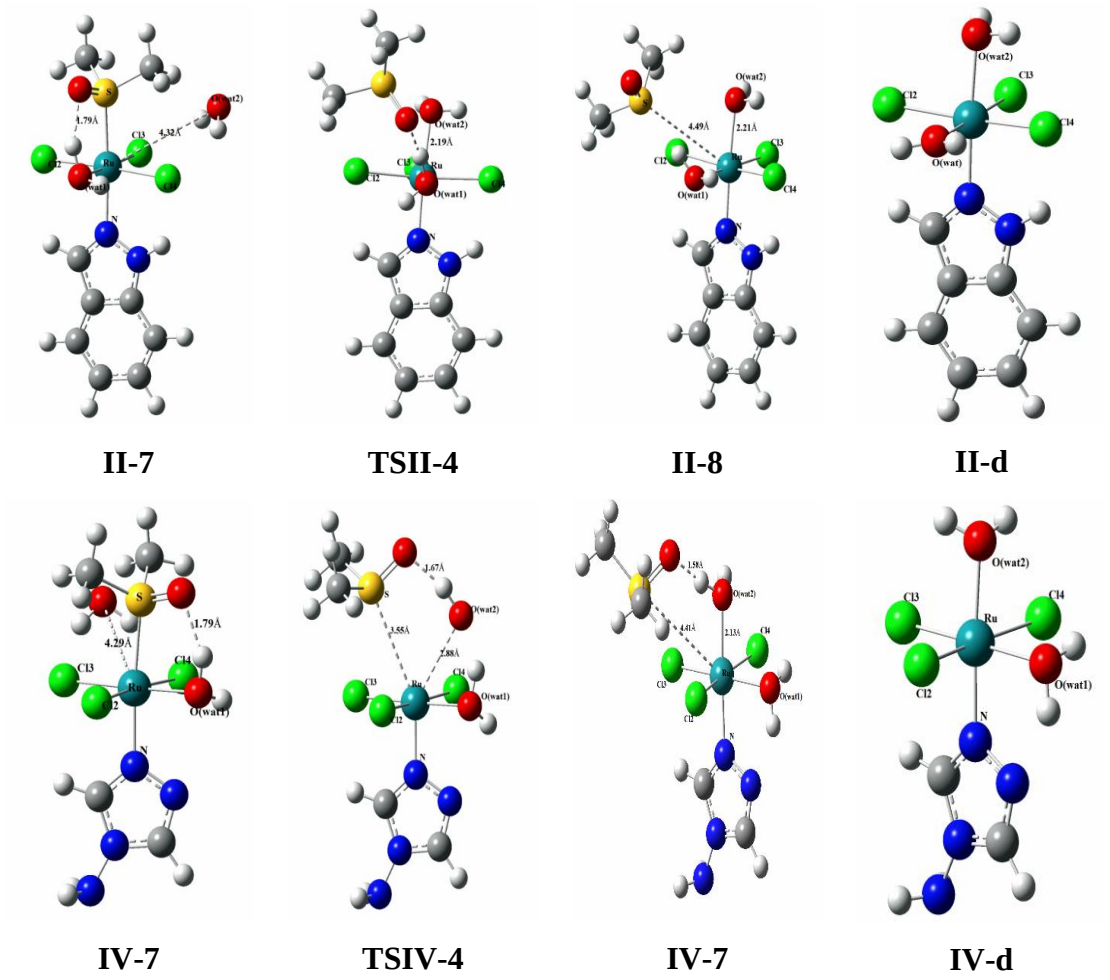

Fig.4.4 Optimized structures for the species involved in the second DMSO hydrolysis of complex **II** and **IV** (path 5).

4.3.3 Reaction Profiles of the Hydrolysis Processes

4.3.3.1 Comparison of first and second step of Cl^- hydrolysis

Change of enthalpies (ΔH) and Gibbs free energies (ΔG) for the hydrolysis reaction of complexes **II** and **IV** in gas and solvent phases calculated at DFT-B3LYP level are presented in Table 4.5 and Table 4.6. It can be observed from Table 4.5 and Table 4.6 that the computed Gibbs free energy in aqueous medium for the path 1 in the hydrolysis reaction of complex **II** and complex **IV** (ΔG =16.94 and 18.80 kcal mol^{-1}) are found to be lower than that of NAMI-A (ΔG =23.2 kcal mol^{-1})[23]. Fig. 4.5 shows the reaction pathway of first and second Cl^- hydrolysis reactions of complex **II** calculated at gas and solvent phases at UB3LYP/(LANL2DZ+6-31G(d,p) level. From Fig. 4.5(a), it is noticed that the activation barrier for path1 is 25.10 kcal mol^{-1} whereas for path 2 and path 3 are found to be 25.73 and 33.26 kcal mol^{-1},

respectively. These observations reveal that hydrolysis mechanism proceeds through path 3 is found to be more difficult than the path 1 and path 2.

Table 4.5 Total ZPE ($E_{tot/ZPE}$), Change of enthalpies (ΔH), Gibbs free energies (ΔG) and entropies (ΔS) at 298.15 K for all intermediate species and transition States of the hydrolysis processes of complex **II**

First Cl^- hydrolysis(path1)					
Species	ΔE_{tot}	$\Delta E_{tot/ZPE}$	ΔH	ΔG	ΔS
II-1	0	0	0	0	0
TSII-1	25.73(20.71)	25.10(18.20)	25.10(18.19)	25.10(16.94)	-1.30(-3.01)
II-2	15.06(9.41)	15.06(10.04)	15.68(9.41)	15.06(9.41)	-1.02(-2.64)
Second Cl^- hydrolysis (Path2)					
II-3	0	0	0	0	0
TSII-2	25.10(24.47)	25.10(23.85)	24.50(23.85)	25.73(24.47)	3.53(3.31)
II-4	8.15(3.75)	7.53(3.77)	6.90(3.14)	8.16(3.77)	3.48(3.50)
Second Cl^- hydrolysis(Path3)					
II-3′	0	0	0	0	0
TSII-2′	32.00(28.24)	32.00(29.49)	30.75(29.49)	33.26(29.49)	6.07(7.98)
II-4′	10.66(6.90)	10.04(6.90)	8.79(5.65)	10.67(8.16)	5.46(8.93)
First DMSO hydrolysis(Path4)					
II-5	0	0	0	0	0
TSII-3	22.59(20.08)	21.34(18.83)	21.34(18.20)	20.71(19.45)	-1.56(4.89)
II-6	6.90(6.90)	6.28(6.28)	6.28(6.28)	3.77(5.65)	-0.90(-1.76)
Second DMSO hydrolysis(Path5)					
II-7	0	0	0	0	0
TSII-4	3.77(0)	3.77(0)	3.77(0.63)	3.14(-1.88)	-3.62(-7.53)
II-8	10.04(6.28)	10.04(6.28)	10.04(6.90)	8.79(3.77)	-4.38(-10.23)

Table 4.6 Total ZPE ($E_{tot/ZPE}$), Change of enthalpies (ΔH), Gibbs free energies (ΔG) and entropies (ΔS) at 298.15 K for all intermediate species and transition States of the hydrolysis processes of complex **IV**

First Cl^- hydrolysis (path1)					
Species	ΔE_{tot}	$\Delta E_{tot/ZPE}$	ΔH^0	ΔG	ΔS^0
IV-1	0	0	0	0	0
TSIV-1	27.61(25.86)	27.61(25.86)	26.36(25.86)	28.24(18.81)	3.54(1.98)
IV-2	5.02(5.02)	5.02(5.02)	4.39(5.02)	5.02(-9.31)	1.10(0.56)
Second Cl^- hydrolysis (Path2)					
IV-3	0	0	0	0	0
TSIV-2	20.71(21.96)	21.33(21.96)	20.08(21.96)	22.59(22.59)	5.96(2.10)
IV-4	1.88(-1.88)	2.51(-1.26)	1.26(-1.25)	3.77(-1.21)	6.68(2.91)
Second Cl^- hydrolysis(Path3)					
IV-3′	0	0	0	0	0
TSIV-2′	(28.24)	25.72(28.24)	25.50(28.24)	26.98(29.49)	5.78(2.09)
IV-4′	(5.65)	-6.27(5.02)	6.12(5.65)	2.44(5.02)	6.23(-3.17)
First DMSO hydrolysis(Path4)					
IV-5	0	0	0	0	0
TSIV-3	20.08(18.83)	18.20(18.20)	18.83(17.57)	17.57(17.57)	7.29(-1.47)
IV-6	5.65(76.56)	5.02(77.18)	6.26(76.56)	3.14(76.56)	8.30(-2.26)
Second DMSO hydrolysis(Path5)					
IV-7	0	0	0	0	0
TSIV-4	17.57(14.43)	17.57(15.06)	16.32(13.18)	16.94(13.80)	-0.058(2.30)
IV-8	1.88(-2.51)	2.51(-2.51)	1.88(-2.51)	1.26(-2.51)	-2.77(-0.18)

The similar sequences of energy barrier heights can also be noticed in Fig. 4.5(b). The computed Gibbs free energies for the formation stationary points involved in hydrolysis reactions follow path 1, Path 2 and path 3 for the complex **II** calculated using CPCM solvation model in aqueous solution have been presented in Fig. 4.5(b). Fig. 4.5(a) and Fig 4.5(b) reveal that, on incorporation of solvent effect decreases the activation barriers of all the steps involves in the hydrolysis of complexes **II** and **IV**. The decrease in activation barriers on incorporation of solvent effect is due to the

solvation of the reactant and intermediate species. Fig. 4.6 presented the computed relative free energies for Cl^- hydrolysis reaction of complex **IV** in gas phase (Fig. 4.6 (a)) as well as in solvent phase (Fig. 4.6 (b)). Fig. 4.6 (b) also suggests that path 3 in the second hydrolysis step is slow in comparison to path 1 and path 2. Energy profile diagram for the hydrolysis of complexes **II** and **IV** indicate that the second hydrolysis leading to the *trans* isomer is comparatively slower than the formation *cis* isomer which is may be due to *trans* effect and hydrogen bonding. Higher *trans* effect of leaving Cl^- ligand than that of incoming water ligand lead to the formation of *cis*-diaqua complexes. Free energy profile diagram Fig. 4.5(b) shows that the proposed three reaction pathways (path1, path 2 and path 3) for the hydrolysis of complex **II** is found to be endothermic by 9.34, 3.77 and 8.16 kcal mol^{-1}. On the other hand, hydrolysis of the first Cl^- and path 2 in the second hydrolysis for the complex **IV** are predicted to be exothermic by 9.31 and 1.21kcal mol^{-1}, while path 3 is endothermic by 5.02 kcal mol^{-1}.

(a) (b)

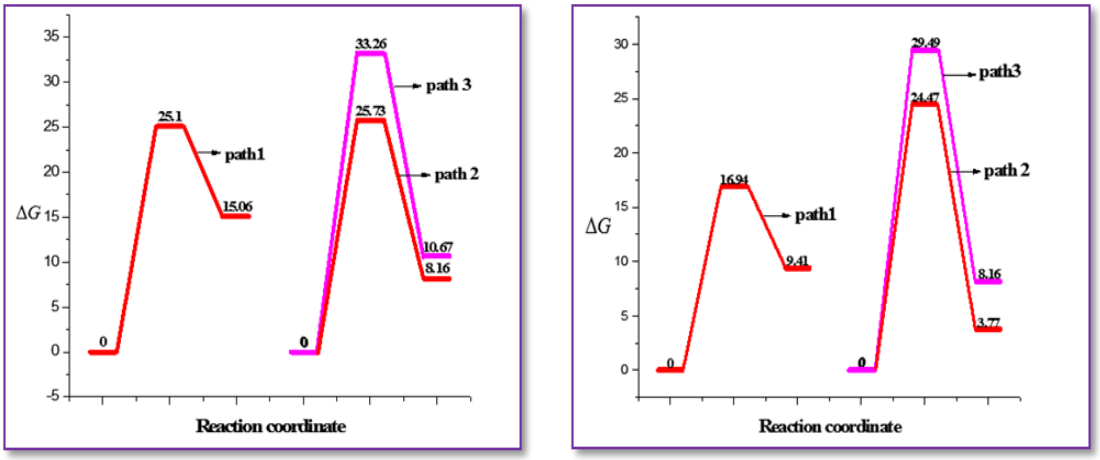

Fig. 4.5 Free energy profile diagram for the first hydrolysis of complex **II** in (a) gas phase and (b) in solvent phase.

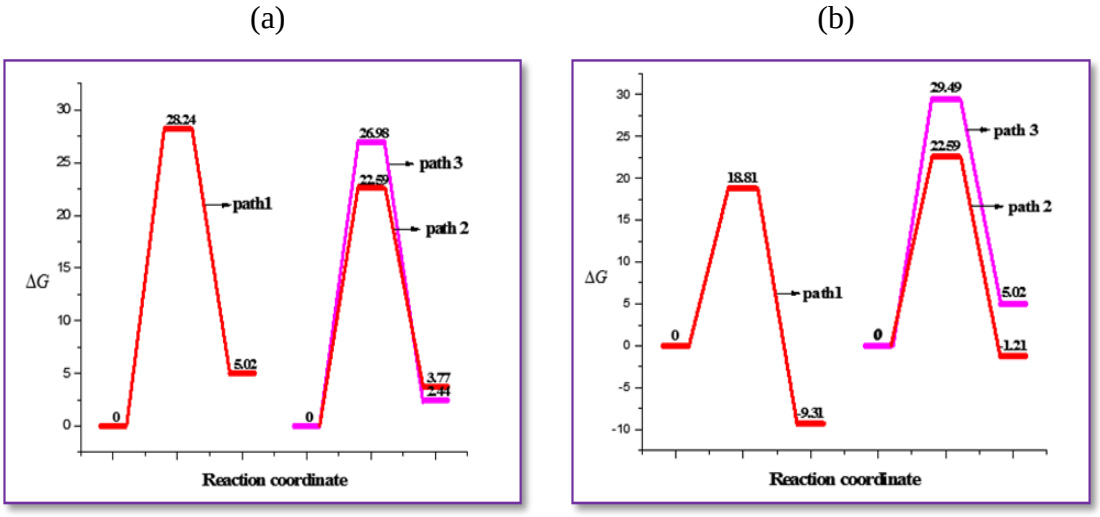

Fig. 4.6 Free energy profile diagram for the first hydrolysis of complex **IV** in (a) gas phase and (b) in solvent phase.

4.3.3.2 Comparison of first step of Cl^- and first step of DMSO hydrolysis

In Fig 4.7, the computed Gibbs free energies for first step of Cl^- hydrolysis (path 1) and DMSO hydrolysis (path 4) of complexes **II** and **IV** are presented for comparison. The activation free energy values for the substitution of Cl^- and DMSO ligands with H_2O molecules of complex **II** are comparable. However, for complex **II** thermodynamically Cl^- dissociation is found to be more favorable than DMSO (Fig. 4.7(a) and Fig. 4.7(b)). In gas phase (Fig. 4.7(a)), the activation energy barrier for path 4 is lower than path 1 indicates that DMSO dissociation occurs easily. On incorporation of water effect the reaction proceeds faster for Cl^- dissociation as the activation free energy values of the second Cl^--water exchange decreases (path 1) compared to DMSO-water exchange *i.e.* path 4 (Fig. 4.7(b)). Further, The larger stability of **II-a** as compared to **II-c** is because of the presence of one intramolecular (DMSO—HOH) hydrogen bond at a distance 1.85 Å, whereas no hydrogen bonding interaction is observed for **II-c**. Hence larger stability favors dissociation of Cl^- ligand. Similar to complex **II**, DMSO substitution is found to be favorable in the gas phase for complex **IV** (Fig. 4.7(a) and Fig. 4.7(c)) but in the solvent phase, different results are obtained for both the complexes (Fig. 4.7(b) and Fig. 4.7(d)). Thus, occurance of DMSO dissociation is found to be difficult and more accurate model in solvent medium is required to design. Thus, both kinetic and thermodynamic parameters evaluated for the hydrolysis of complexes **II** and **IV** suggest that

substitution of chloro ligand is more favorable. Results derived in this investigation are in agreement with the available experimental and theoretical results.[23, 41]

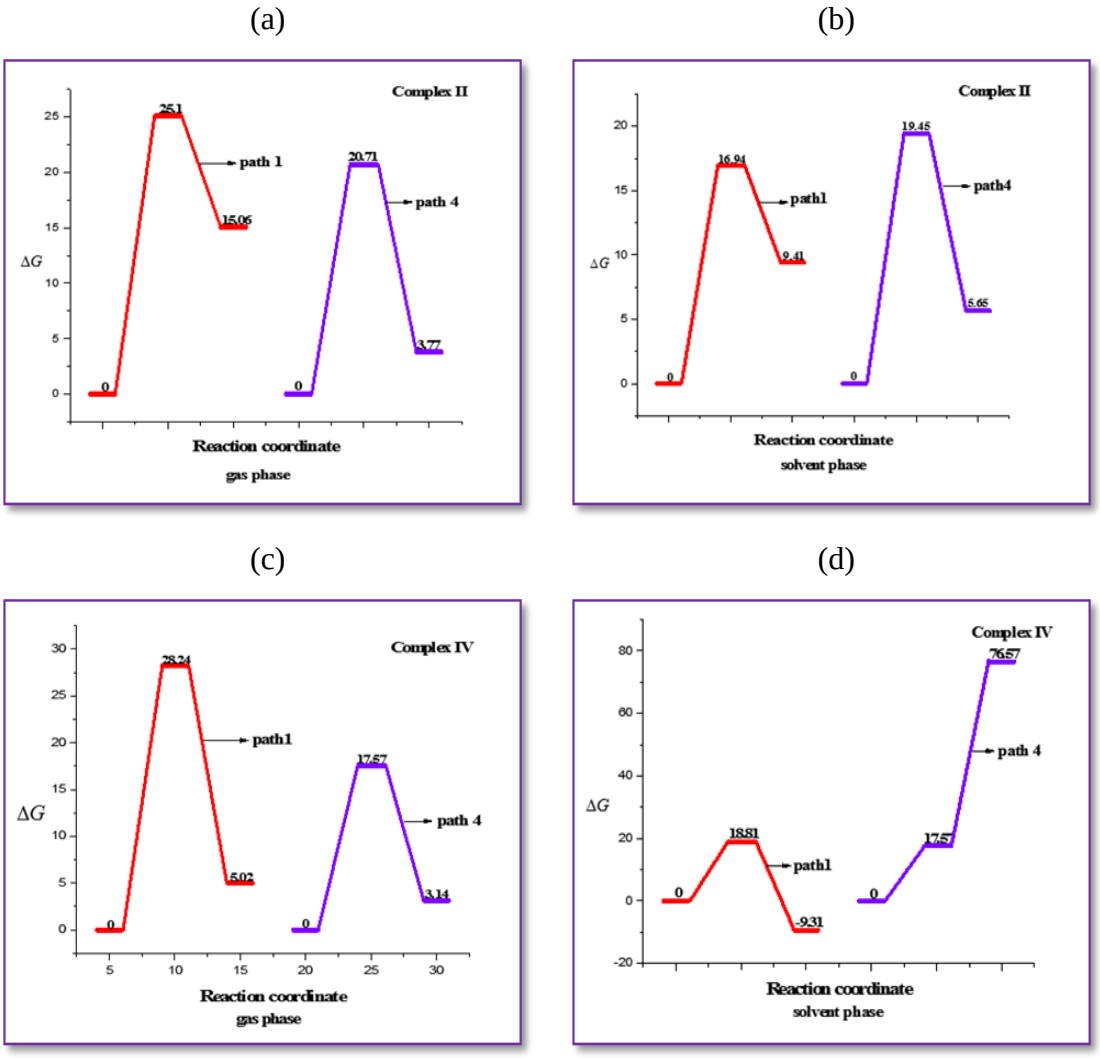

Fig. 4.7 Free energy profiles of Cl^- (path 1) and DMSO (path 4) hydrolysis of complexes **II** and **IV**.

4.3.3.3 Comparison of second step of Cl^- and DMSO hydrolysis

The free energy profiles for the second step of Cl^- and DMSO hydrolysis of complexes **II** and **IV** computed in the gas and solvent phases are displayed in Fig. 4.8. The analysis of the second hydrolysis reaction reveals interesting features. Fig. 4.8(a) and Fig. 4.8(b) show that similar to the previous step, in second step, DMSO dissociation becomes kinetically unlikely with respect to that of Cl^-. But in case of complex **IV** opposite results are obtained, *i.e.*, dissociation of neutral DMSO ligand is favored with respect to the Cl^- ligand, yet product **IV-b** stability (stabilized by a hydrogen bonding) favors Cl^- dissociation.

Since the 20th century the hydrolysis process of platinum based anticancer complexes has been investigated and the theoretical methods and models are well established. But the theoretical study is newer in the case of ruthenium complexes, hence to explore and design more accurate solvent model for the hydrolysis of NAMI-A and NAMI type of complexes is a very difficult task. During the investigation of hydrolysis mechanism of complexes **II** and **IV**, second step of DMSO hydrolysis is found to be very complicated and different results are obtained. However, our present quantum chemical studies provide some aspects which may be helpful in understanding the reaction mechanism of these complexes with the biomolecular target.

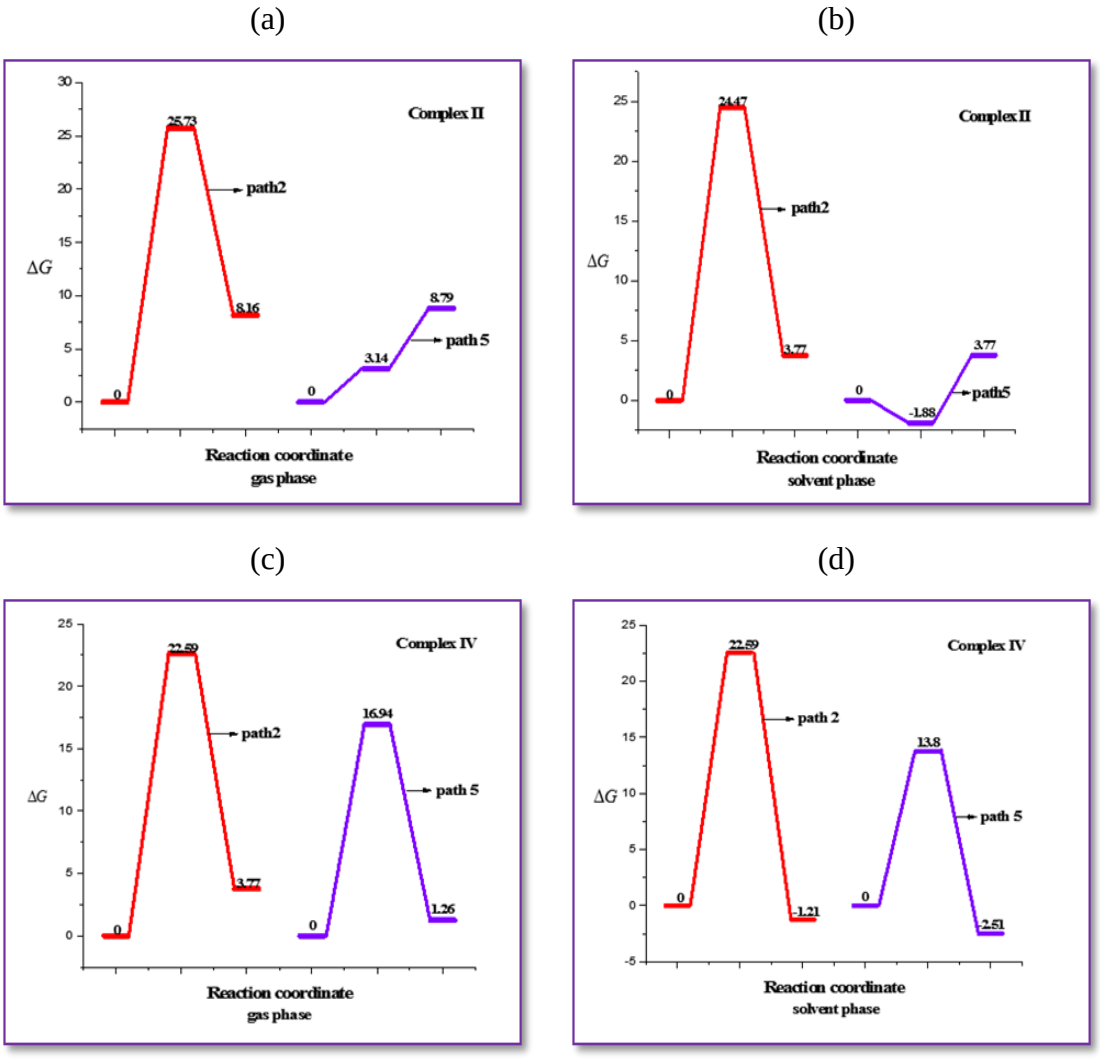

Fig. 4.8 Free energy profile diagram for the second step of Cl^- (path 2) and DMSO (path 4) hydrolysis reaction of complexes **II** and **IV**.

4.4 Conclusion

In this chapter, we have investigated detail hydrolysis mechanism of complex **II** and complex **IV** using density functional theory method. The stationary points formed during the course of hydrolysis reveal pseudooctahedral geometries and follow interchange dissociative mechanism. The computed Gibbs free energies (ΔG) in aqueous medium for the replacement of one chloro ligand with aqua ligand from the complexes **II** and **IV** are found to be 16.94 and 18.81 kcal mol^{-1}. Substitution of second Cl^- ligand with water molecule through path 2 proceed more favorably, i.e., the kinetic preference for the formation of *cis*-diaqua ruthenium complexes. Calculated thermodynamic parameters suggest the replacement of one Cl^- ion from the complexes **II** and **IV** are more favorable in comparison to DMSO substitution. For the second hydrolysis step of DMSO dissociation, some disagreement still exists, since different results are obtained for the two complexes and thus more accurate solvent model needs to be designed. Present study suggests that first step of hydrolysis for the complexes **II** and **IV** occur mainly by the substitution chloro ligand and then follow path 2 for the second step of hydrolysis.

References

1. D. Frasca, J. Ciampa, J. Emerson, R. S. Umans, M. J. Clarke, *Met.-Based Drugs*, 1996, **3**, 197-209.
2. W. H. Ang, P. J. Dyson, *Eur. J. Inorg. Chem*., 2006, 4003-4018.
3. V. Brabec, O. Novakova, *Drug Resist. Update*, 2006, **9**, 111-122.
4. C. S. Allardyce, P. J. Dyson, *Platinum Met. Rev*., 2001, **45**, 62-69.
5. G. Sava, A. Bergamo, S. Zorzet, B. Gava, C. Casarsa, M. Cocchietto, A. Furlani, V. Scarcia, B. Serli, E. Iengo, E. Alessio, G. Mestroni, *Eur. J. Cancer*, 2002, **38**, 427-435.
6. M. Bouma, B. Nuijen, M. T. Jansen, G. Sava, A. Flaibani, A. Bult, J. H. Beijnen, *Int. J .Phar*., 2002, **248**, 239-246.
7. A. Vacca, M. Bruno, A. Boccarelli, M. Coluccia, D. Ribatti, A. Bergamo, S. Garbisa, L. Sartor, G. Sava, *Br. J. Cancer*, 2002, **86**, 993-998.
8. S. Pacor, S. Zorzet, M. Cocchietto, M. Bacac, M. Vadori, C. Turrin, B. Gava, A. Castellarin, G. Sava, *J. Pharmacol. Exp. Ther*., 2004, **310**, 737-744.
9. M. Howe-Grant, S. Lippard, *J. Metal Ions Biol. Syst*., 1980, **11**, 63-125.
10. M. Pavelka, M. F. A. Lucas, N. Russo, *Chem. Eur. J*., 2007, **13**, 10108-10116.
11. S. Suvachittanont, R. van Eldik, *Inorg. Chem*., 1994, **33**, 895-899.
12. S. Suvachittanont, H. Hohmann, R. van Eldik, J. Reedijk, *J. Inorg. Chem*., 1993, **32**, 4544-4548.
13. H. Hohmann, B. Hellquist, R. Van Eldik, *Inorg. Chem*., 1992, **31**, 1090-1095.
14. E. Holler, W. Schaller, B. K. Keppler, *Arzneim.-Forsch., Drug Res*., 1991, **41**, 1065.
15. L. Messori, F. Kratz, E. Alessio, *Met. Based Drugs*, 1996, **3**, 1-9.
16. M. J. Clarke, F. Zhu, D. R. Frasca, *Chem. Rev*., 1999, **99**, 2511-2533
17. G. Sava, E. Alessio, A. Bergamo, G. Mestroni, *In Biological Inorganic Chemistry*; M.J.Clarke, P.J. Sadler, *Eds. Springer-Verlag: Berlin*, 1999,**1**, pp.154.
18. A. Kung, T. Pieper, R. Wissiack, E. Rosenberg, B. K. Keppler, *J. Biol. Inorg. Chem*., 2001, **6**, 292-299.
19. O. M. Ni Dhubhghaill, W. R. Hagen, B. K. Keppler, K. G. Lipponer, P. J. Sadler, *Dalton Trans*., 1994, **22**, 3305-3310.
20. C. Anderson, A. L. Beauchamp, *Can. J. Chem*., 1995, **73**, 471-482.

21. J. C. Chen, J. Li, L. Qian, K. C. Zheng, *J. Mol. Struct.(THEOCHEM)*, 2005, **728**, 93-101.

22. C. Scolaro, T. J. Geldbach, S. Rochat, A. Dorcier, C. Gossens, A. Bergamo, M. Cocchietto, I. Tavernelli, G. Sava, U. Rothlisberger, P. J. Dyson, *Organometallics*, 2006, **25**, 756-765.

23. J. C. Chen, L. M. Chen, S. Y. Liao, K. C. Zheng, L. N. Ji, *J Phys. Chemi. B*, 2007, **111**, 7862-7869.

24. J. C. Chen, L. M. Chen, S. Y. Liao, K. C. Zheng, L. N. Ji, *Dalton Trans*, 2007, **32**, 3507-3515.

25. J. C. Chen, L. M. Chen, S. Y. Liao, K. C. Zheng, L. N. Ji, *J. Mol. Struct.(THEOCHEM)*, 2009, **901**, 137-144.

26. J. C. Chen, L. M. Chen, S. Y. Liao, K. C. Zheng, L. N. Ji, *Phys. Chem. Chem. Phys*., 2009, **11**, 3401-3410.

27. J. C. Chen, L. M. Chen, S. Y. Liao, K. C. Zheng, L. N. Ji, *Int. J. Quantum Chem*., 2010, **110**, 1252-1263.

28. N. Besker, C. Coletti, A. Marrone, N. Re, *J. Phys. Chem. B*, 2008, **112**, 3871-3875.

29. A. V. Vargiu, A. Robertazzi, A. Magistrato, P. R. Paolo Carloni, *J. Phys. Chem. B*, 2008, **112**, 4401-4409.

30. V. Barone, M. Cossi, *J. Phys. Chem. A*, 1998, 1995.

31. M. J. Frisch, G. W. Trucks, H. B. Schlegel, G. E. Scuseria, M. A. Robb, J. R. Cheeseman, G. Scalmani, V. Barone, B. Mennucci, G. A. Petersson, H. Nakatsuji, M. Caricato, X. Li, H. P. Hratchian, A. F. Izmaylov, J. Bloino, G. Zheng, J. L. Sonnenberg, M. Hada, M. Ehara, K. Toyota, R. Fukuda, J. Hasegawa, M. Ishida, T. Nakajima, Y. Honda, O. Kitao, H. Nakai, T. Vreven, J . A. Montgomery, J. E. Peralta, F. Ogliaro, M. Bearpark, J. J. Heyd, E. Brothers, K. N. Kudin, V. N. Staroverov, T. Keith, R. Kobayashi, J. Normand, K. Raghavachari, A. Rendell, J. C. Burant, S. S. Iyengar, J. Tomasi, M. Cossi, N. Rega, J. M. Millam, M. Klene, J. E. Knox, J. B. Cross, V. Bakken, C. Adamo, J. Jaramillo, R. Gomperts, R. E. Stratmann, O. Yazyev, A. J. Austin, R. Cammi, C. Pomelli, J. W. Ochterski, R. L. Martin, K. Morokuma, V. G. Zakrzewski, G. A. Voth, P. Salvador, J. J. Dannenberg, S. Dapprich, A. D.

Daniels, O. Farkas, J. B. Foresman, J. V. Ortiz, J. Cioslowski, D. J. Fox, Gaussian 09 (Revision B.01), Gaussian Inc., Wallingford, CT, 2010.

32. C. Lee, W. Yang, R. G. Parr, *Phys Rev*., 1988, **37**, 785-789.

33. P. J. Hay, W. R. Wadt, *J. Chem. Phys*., 1985, **82**, 270-284.

34. J. P. Perdew, K. Burke, Y. Wang, *Phys. Rev. B*, 1996, **54**, 16533-16539.

35. C. Gonzalez, H. B. Schlegel, *J. Chem. Phys*., 1989, **90**, 2154-2161.

36. C. Gonzalez, H. B. Schlegel, *J. Phys. Chem*., 1990, **94**, 5523-5527.

37. D. V. Deubel, J. K. C. Lau, *Chem. Commun*., 2006, 2451-2453.

38. J. K. C. Lau, D. V. Deubel, *J. Chem. Theory Comput*., 2006, **2**, 103.

39. V. Barone, M. Cossi, *J. Phys. Chem. A*, 1998, **102**, 1995-2001.

40. E. Alessio, G. Mestroni, A. Bergamo, G. Sava, *Met. Ions Biol.Syst*., 2004, **42**, 323-351.